Hindawi Publishing Corporation
International Journal of Photoenergy
Volume 2014, Article ID 392394, 14 pages
http://dx.doi.org/10.1155/2014/392394

Research Article

Buck-Boost/Forward Hybrid Converter for PV Energy Conversion Applications

Sheng-Yu Tseng, Chien-Chih Chen, and Hung-Yuan Wang

Department of Electrical Engineering, Chang-Gung University, 259 Wen-Hwa 1st Road, Tao-Yuan 333, Taiwan

Correspondence should be addressed to Sheng-Yu Tseng; sytseng@mail.cgu.edu.tw

Received 16 August 2013; Revised 28 February 2014; Accepted 28 February 2014; Published 7 April 2014

Academic Editor: Ismail H. Altas

This paper presents a charger and LED lighting (discharger) hybrid system with a PV array as its power source for electronic sign indicator applications. The charger adopts buck-boost converter which is operated in constant current mode to charge lead-acid battery and with the perturb and observe method to extract maximum power of PV arrays. Their control algorithms are implemented by microcontroller. Moreover, forward converter with active clamp circuit is operated in voltage regulation condition to drive LED for electronic sign applications. To simplify the circuit structure of the proposed hybrid converter, switches of two converters are integrated with the switch integration technique. With this approach, the proposed hybrid converter has several merits, which are less component counts, lighter weight, smaller size, and higher conversion efficiency. Finally, a prototype of LED driving system under output voltage of 10 V and output power of 20 W has been implemented to verify its feasibility. It is suitable for the electronic sign indicator applications.

1. Introduction

In recent years, light emitting diodes (LEDs) are becoming more prevalent in a wide application. Due to material advances over the past few decades, efficiencies of LEDs have increased many times [1], and their applications have rapidly grown for automotive taillights, LCD back lights, traffic signals, and electronic signs [2, 3]. Moreover, serious greenhouse effect and environmental pollution caused by overusing fossil fuels have disturbed the balance of global climate. In order to reduce emission of exhausted gases, zero-emission renewable energy sources have been rapidly developed. One of these sources is photovoltaic (PV) arrays, which is clean and quiet and an efficient method for generating electricity. As mentioned above, this paper proposes an LED driving system, which adopts the PV arrays for electronic sign applications.

In electronic sign applications using PV arrays, the power system will inevitably need batteries for storing energy during the day and for releasing energy to LED lighting during the night. Therefore, it needs a charger and discharger (LED driving circuit), as shown in Figure 1. Since the proposed power system belongs to the low power level applications, buck, boost, buck-boost, flyback, or forward converter is more applied to the proposed one [4–12]. In these circuit structures, according to the relationships among PV output voltage V_{PV}, battery voltage V_B, and output voltage V_O, the proposed hybrid converter can choose functions, which are of step-up and -down simultaneously as the charger or discharger for a wider application. Due to the previously described reasons, the charger of the proposed one adopts buck-boost converter and the discharger uses forward converter. Moreover, since forward converter exits two problems, which are the energies trapped in leakage inductor and magnetizing inductor of transformer T_f, it needs a snubber or circuit to recover these energies. Therefore, forward converter can use an active clamp circuit to solve these problems. In order to simplify the proposed hybrid converter and increase its conversion efficiency, a bidirectional buck-boost converter and active clamp forward converter are used, as shown in Figure 2. Since charger and discharger (LED driving circuit) of the proposed hybrid converter are operated in complement and they use switch S_1 to control their operational states, inductor L_1 of buck-boost converter and magnetizing inductor L_m of transformer T_f can be merged. Therefore, switches of the bidirectional buck-boost converter and active clamp forward

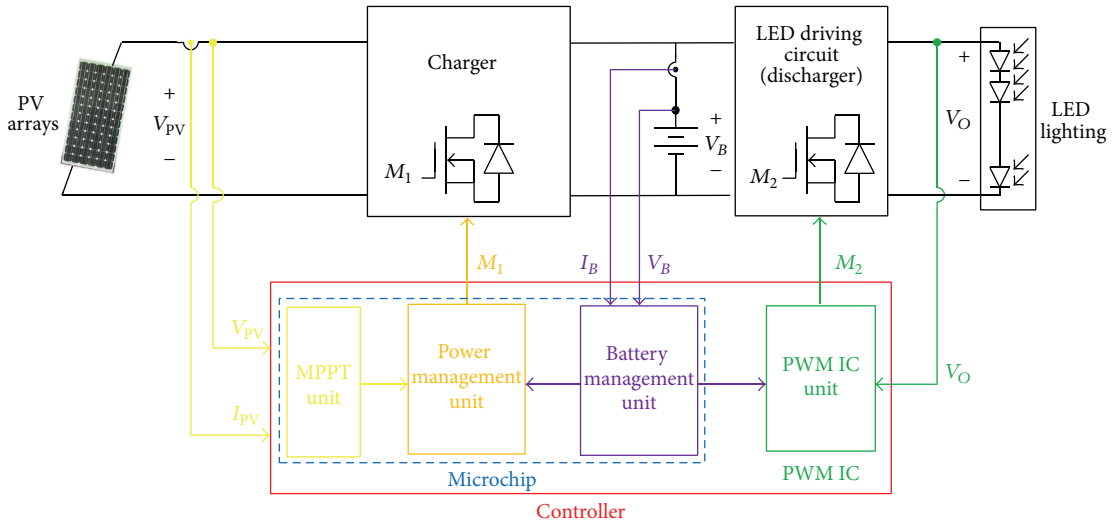

FIGURE 1: Block diagram of the proposed hybrid converter for electronic sign applications.

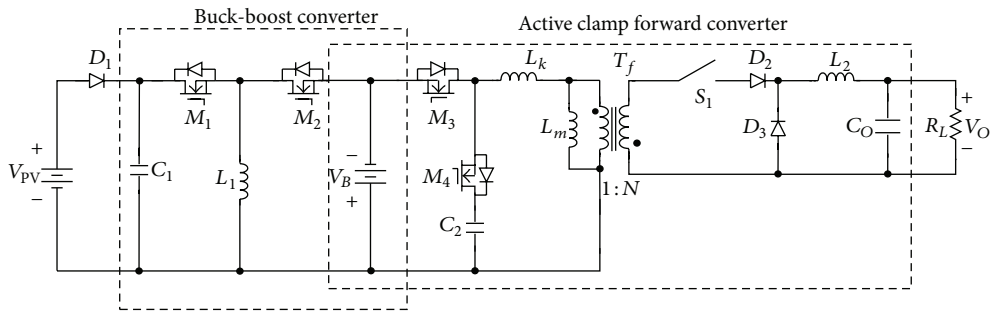

FIGURE 2: Schematic diagram of the hybrid converter for electronic sign applications.

converter are integrated with synchronous switch technique [13] to reduce their component counts, as shown in Figure 3. With this circuit structure, the proposed one can yield higher efficiency, reduce weight, size, and volume and increase the discharging time of battery under the same storing energy, significantly.

The proposed hybrid converter using PV arrays supplies power to LED lighting for electronic sign applications. The proposed one includes charger and discharger. Since the proposed one uses PV arrays as its power source, it must be operated at the maximum power point (MPP) of PV arrays to extract its maximum power. Many maximum power point tracking (MPPT) methods of PV arrays have been proposed [14–21]. They are, respectively, power matching [14, 15], curve-fitting [16, 17], perturb-and-observe [18, 19], and incremental conductance [20, 21] methods. Since power matching method requires a specific insolation condition or load, it will limit its applications. MPPT using curve-fitting technique needs prior establishment characteristic curve of PV arrays. It cannot predict the characteristics including other factors, such as aging, temperature, and a possible breakdown of individual cell. The incremental conductance technique requires an accurate mathematical operation. Its controller is more complex and higher cost. Due to a simpler control and lower cost of perturb and observe method, the proposed hybrid converter adopts the perturb and observe method to implement MPPT.

For electronic sign applications using LED, the power system needs battery to store energy during day and to discharge energy for driving LED during night. In order to generate better performances of battery charging, many battery charging methods have been proposed. They are constant trickle current (CTC), constant current (CC), and CC and constant-voltage (CC-CV) hybrid charge methods [22]. Among these methods, the CTC charging method needs a larger charging time. Battery charging using CC-CV method requires to sense battery current and voltage, resulting in a more complex operation and higher cost. Due to a simpler controller of battery charger using CC charging method, it is adopted in the proposed hybrid converter. According to description above, the proposed hybrid converter uses the perturb and observe method to track MPP of PV arrays and

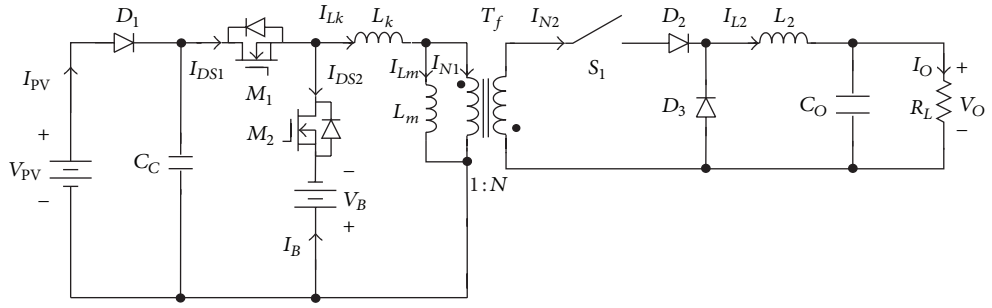

Figure 3: Schematic diagram of the proposed hybrid converter for electronic sign applications.

adopts the CC charging method to simplify battery charging. All overall power system can achieve battery charging and LED driving.

2. Circuit Structure Derivation of the Proposed Hybrid Converter

The hybrid converter consists of a bidirectional buck-boost and active clamp forward converter, as shown in Figure 2. Due to complementary operation between two converters, two switch pairs of (M_1, M_4) and (M_2, M_3) can be operated in synchronous. It will do not affect the operation of the proposed original converter. Since switch pairs of (M_2, M_3) has a common node, they meet the requirements of switch integration technique [11]. According to principle of switch integration technique, switches M_2 and M_3 can be merged, as shown in Figure 4(a). Since charger and LED driving circuit (discharger) are operated in complementary, switch M_2 and M_3 are also regarded as an independent operation. Therefore, voltages across switches M_2 and M_3 are the same value in each operation state. Diode D_{F231} and D_{F232} can be removed, while diode D_{B231} and D_{B232} can be shorted, as shown in Figure 4(b). In Figure 4(b), since $L_K \ll L_m$, L_K can be neglected. The inductor L_1 and magnetizing L_m are connected in parallel. Although features of inductors L_1 and L_m are different, their design rules are to avoid them to operate in saturation condition. Therefore, they can be merged as inductor L_{1m}, as shown in Figure 4(c).

From Figure 4(c), it can be seen that switch M_1 and M_4 have a common node. They can use switch integration technique to combine them, as shown in Figure 4(d). Since voltages across M_1 and M_4 are the same values, diodes D_{B141} and D_{B142} are shorted and diodes D_{F141} and D_{F142} can be removed, as shown in Figure 4(e). From Figure 4(e), it can be found that capacitors C_1 and C_2 are connected in parallel. They can be integrated as capacitor C_C, as illustrated in Figure 4(f). To simplify symbols of components illustrated in Figure 4(f), component symbols will be renamed, as shown in Figure 3. Note that switch S_1 can be operated by manual or automatic method to control the operational states of the proposed hybrid converter.

Buck-boost and forward converters are combined to form the proposed hybrid converter. Since operation of buck-boost converter is the same as the conventional buck-boot converter, its operational principle is described in [8]. It will not be described in this paper. The forward converter with the active clamp circuit recovers the energies stored in magnetizing and leakage inductors of transformer T_f and achieves zero-voltage switch (ZVS) at turn-on transition for switches M_1 and M_2. It operational mode can be divided into 9 modes and their Key waveforms are illustrated in Figure 5, since their operational modes are similar to those modes of the conventional converter illustrated in [23]. It is also not described in this paper.

3. Design of the Proposed Hybrid Converter

The proposed hybrid converter consists of buck-boost converter and active clamp forward converter. Since switches and inductors in two converters are integrated with the synchronous switch technique, design of the proposed one must satisfy requirements of each converter. Since design of the active clamp forward converter is illustrated in [23], buck-boost converter is only analyzed briefly in the following.

3.1. Buck-Boost Converter. Since buck-boost converter is regarded as the battery charger under constant current charging. Its design consideration is to avoid a completely saturation of inductor. Therefore, duty ratio D_{11} and inductor L_m are analyzed in the following.

3.1.1. Duty Ratio D_{11}. Within charging mode, since battery voltage V_B is regarded as a constant voltage during a switching cycle of the proposed hybrid converter, maximum duty ratio $D_{11(\max)}$ of the proposed one can be determined by volt-second balance of inductor L_m. Its relationship is expressed as

$$V_{\mathrm{PV}(\min)} D_{11(\max)} T_s + \left(-V_{B(\max)}\right)\left(1 - D_{11(\max)}\right) T_s = 0, \tag{1}$$

where $V_{\mathrm{PV}(\min)}$ is the minimum output voltage of PV arrays, $V_{B(\max)}$ is the maximum voltage across battery, and T_s represents the period of the proposed hybrid converter. From (1), it can be found that $D_{11(\max)}$ can be illustrated by

$$D_{11(\max)} = \frac{V_{B(\max)}}{V_{\mathrm{PV}(\min)} + V_{B(\max)}}. \tag{2}$$

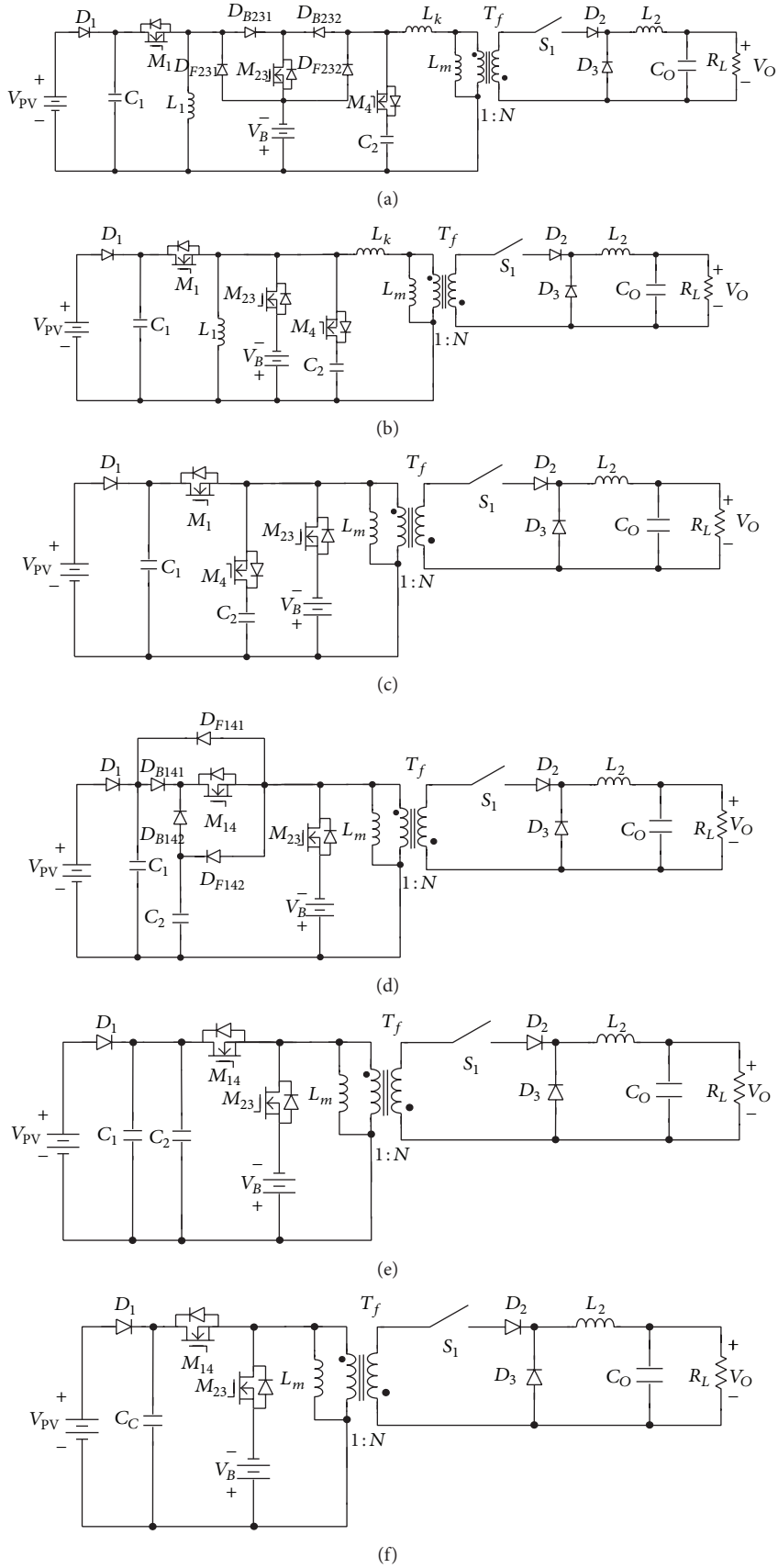

Figure 4: Derivation of the proposed hybrid converter for battery charger.

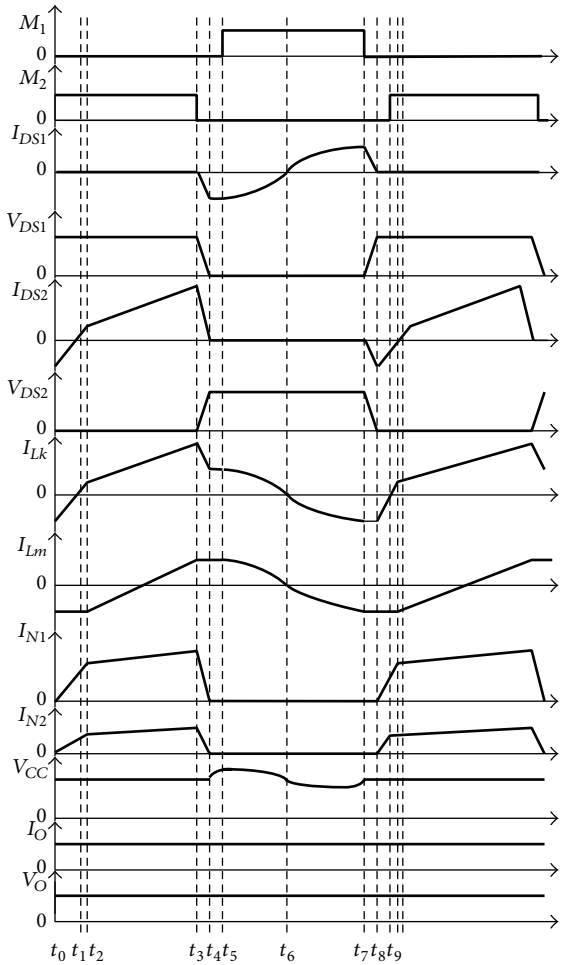

Figure 5: Key waveforms of forward converter with active clamp circuit over one switching cycle.

Moreover, transfer ratio $M_{11(\max)}$ can be also determined as follows:

$$M_{11(\max)} = \frac{D_{11(\max)}}{1 - D_{11(\max)}}. \tag{3}$$

When type of battery is chosen, its maximum charging current $I_{B(\max)}$ is also determined. The charging current I_B can be changed from its maximum charging current $I_{B(\max)}$ to 0 by variation duty ratio D_{11} of switch M_1.

3.1.2. Inductor L_m. Since the proposed hybrid converter is operated in CCM to obtain the maximum charging current $I_{B(\max)}$, its conceptual waveforms of inductor current I_{Lm} and charging current I_B are illustrated in Figure 6. If the proposed one is operated in the boundary of discontinuous conduction mode (DCM) and CCM, the charging current I_B is expressed by

$$I_{B(\mathrm{av})} = \frac{(1 - D_{11})^2 V_B T_s}{2L_{mB}}, \tag{4}$$

where L_{mB} is the inductance L_m at the boundary condition. According to (4), variation of duty ratio D_{11} can obtain

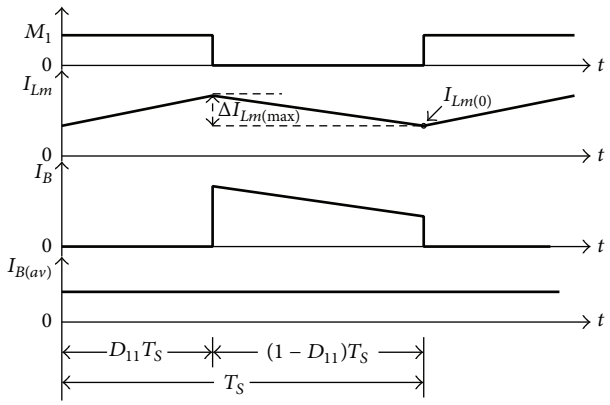

Figure 6: Conceptual waveforms of inductor current I_{Lm} and charging current I_B in buck-boost converter.

a different charging current I_B. In general, the maximum charge current $I_{B(\mathrm{av})\max}$ occurs at the maximum battery voltage $V_{B(\max)}$ and the maximum output voltage $V_{\mathrm{PV}(\max)}$ of PV arrays. Therefore, the boundary inductor L_{mB} can be determined by

$$I_{B(\mathrm{av})\max} = \frac{(1 - D_{11B})^2 V_{B(\max)} T_s}{2L_{mB}}, \tag{5}$$

where D_{11B} is duty ratio of switch M_1 under $V_{B(\max)}$ and $V_{\mathrm{PV}(\max)}$. From (5), it can be found that the maximum boundary inductor $L_{mB(\max)}$ can be expressed as

$$L_{mB(\max)} = \frac{(1 - D_{11B})^2 V_{B(\max)} T_s}{I_{B(\mathrm{av})\max}}. \tag{6}$$

Since the proposed hybrid converter is operated in CCM, inductor L_m must be greater than $L_{mB(\max)}$. Therefore, when $V_{\mathrm{PV}(\max)}$, $V_{B(\max)}$, $I_{B(\mathrm{av})\max}$, and T_s are specified, the minimum inductance $L_{m(\min)}$ $(=L_{mB(\max)})$ can be determined.

In order to avoid the core of transformer T_f operated in saturation state, the working flux density $B_{\max}$ must be less than the saturation flux density B_{sat} of core. Since $B_{\max}$ is proportional to the maximum inductor current $I_{Lm(\mathrm{peak})}$, $I_{Lm(\mathrm{peak})}$ must be first determined. In Figure 6, $I_{Lm(\mathrm{peak})}$ can be expressed as

$$I_{Lm(\mathrm{peak})} = I_{Lm(0)} + \Delta I_{Lm(\max)}, \tag{7}$$

where $I_{Lm(0)}$ is the initial value of inductor current I_{Lm} operated in CCM and $\Delta I_{Lm(\max)}$ represents its maximum variation value. In general, its maximum value $\Delta I_{Lm(\max)}$ can be determined by

$$\Delta I_{Lm(\max)} = \frac{V_{\mathrm{PV}(\max)} D_{11R} T_s}{L_m}, \tag{8}$$

where D_{11R} represents the duty ratio of switch M_1 under $V_{\mathrm{PV(max)}}$ and $V_{B(\max)}$. Furthermore, the maximum charging current $I_{B(\mathrm{av})\max}$ can be expressed as

$$I_{B(\mathrm{av})\max} = \frac{(1 - D_{11R})}{2}\left(I_{Lm(\mathrm{peak})} + I_{Lm(0)}\right) = \frac{(1 - D_{11R})}{2}\left(2I_{Lm(0)} + \frac{V_{\mathrm{PV(max)}} D_{11R} T_s}{L_m}\right). \quad (9)$$

From (9), the initial value $I_{Lm(0)}$ can be determined as follows:

$$I_{Lm(0)} = \frac{I_{B(\mathrm{av})\max}}{1 - D_{11R}} - \frac{V_{\mathrm{PV(max)}} D_{11R} T_s}{2L_m}. \quad (10)$$

From (7), (8), and (10), $I_{Lm(\mathrm{peak})}$ can be denoted as

$$I_{Lm(\mathrm{peak})} = \frac{I_{B(\mathrm{av})\max}}{1 - D_{11R}} + \frac{V_{\mathrm{PV(max)}} D_{11R} T_s}{2L_m}. \quad (11)$$

According to datasheet of core which is supplied by core manufacturer, the number of turns N_1 on the primary side of transformer T_f can be obtained by

$$N_1 = \sqrt{\frac{L_m}{A_L}}, \quad (12)$$

where A_L represents nH per turns^2. That is, $L_m = N_1^2 A_L$. By applying Faraday's law, $B_{\max}$ can be determined as

$$B_{\max} = \frac{L_m I_{Lm(\mathrm{peak})} \times 10^4}{N_1 A_c}, \quad (13)$$

where A_c is the effective cross-section area of the transformer core. In order to avoid saturation condition of core, $B_{\max}$ must be less than saturation flux density B_{sat} of core.

Table 1: Parameter definitions of control signals shown in Figure 4.

Symbol	Definition
V_{PV}	Output voltage of PV arrays
I_{PV}	Output current of PV arrays
P_P	Maximum power of PV arrays
P_B	Charging power of battery ($P_B = V_B I_B$)
$P_{B(\max)}$	Maximum charging power of battery ($P_{B(\max)} = V_B I_{B(\max)}$)
I_B	Charging current of battery
V_B	Battery voltage
V_O	Output voltage of forward converter
I_O	Output current of forward converter
$V_{B(\max)}$	Maximum voltage of battery
$V_{B(\min)}$	Minimum voltage of battery
$V_{O(\max)}$	Maximum output voltage of forward converter
$I_{O(\max)}$	Maximum output current of forward converter
$I_{B(\max)}$	Maximum current of battery
V_{ref}	Reference voltage for obtaining the desired output voltage V_O
I_C	Current command for obtaining the desired charging current I_B
S_M	Control signal of operational mode (S_M = 0, battery charging; S_M = 1, LED driving)
S_n	Insolation level judgment (S_n = 1, low insolation level; S_n = 0, high insolation level)
V_f	Feedback signal of PWM IC
V_e	Error value
G_1, G_2	pwM signals
M_1, M_2	Gate signals of switches M_1 and M_2

4. Configuration of the Proposed PV Hybrid Converter

Since the proposed PV power system includes charger and discharger and adopts PV arrays as its power source, its circuit structure and control algorithm are described in the following.

4.1. Circuit Structure of the Proposed PV Power System. The proposed PV power system consists of battery charger, LED driving circuit (discharger), and controller, as shown in Figure 1. The battery charger and LED driving circuit using buck-boost and active clamp forward hybrid converter are shown in Figure 3. In addition, controller adopts microchip and PWM IC for managing battery charging and LED driving circuit. The microchip is divided into 3 units (MPPT, power management, and battery management units) to implement MPPT of PV arrays and battery charging. The PWM IC is used to regulate output voltage of LED driving circuit. In the microchip of the controller, the MPPT unit senses PV voltage V_{PV} and current I_{PV} to achieve MPPT, which adopts perturb and observe method. The battery management unit acquires battery voltage V_B and current I_B for implementing CC charging of battery. Since the proposed hybrid converter is required to match MPPT of PV arrays and CC charging mode, the power management unit can manage the power flow between PV arrays and battery, depending on the relationship of the generated power of PV arrays and the required power of battery charging. All of protections are implemented by microchip. The protections include overcurrent and overvoltage protections of the proposed hybrid converter and undercharge and overcharge of battery. Therefore, the proposed one can achieve the optimal utility rate of PV arrays and a better performance of battery charging.

4.2. Control Algorithm of the Proposed Hybrid Converter. In Figure 1, the controller of the proposed hybrid converter includes microchip and PWM IC to achieve battery charging and LED driving. In order to implement battery charging and LED driving, block diagram of the hybrid converter is shown in Figure 7. In Figure 7, control signals are defined in Table 1.

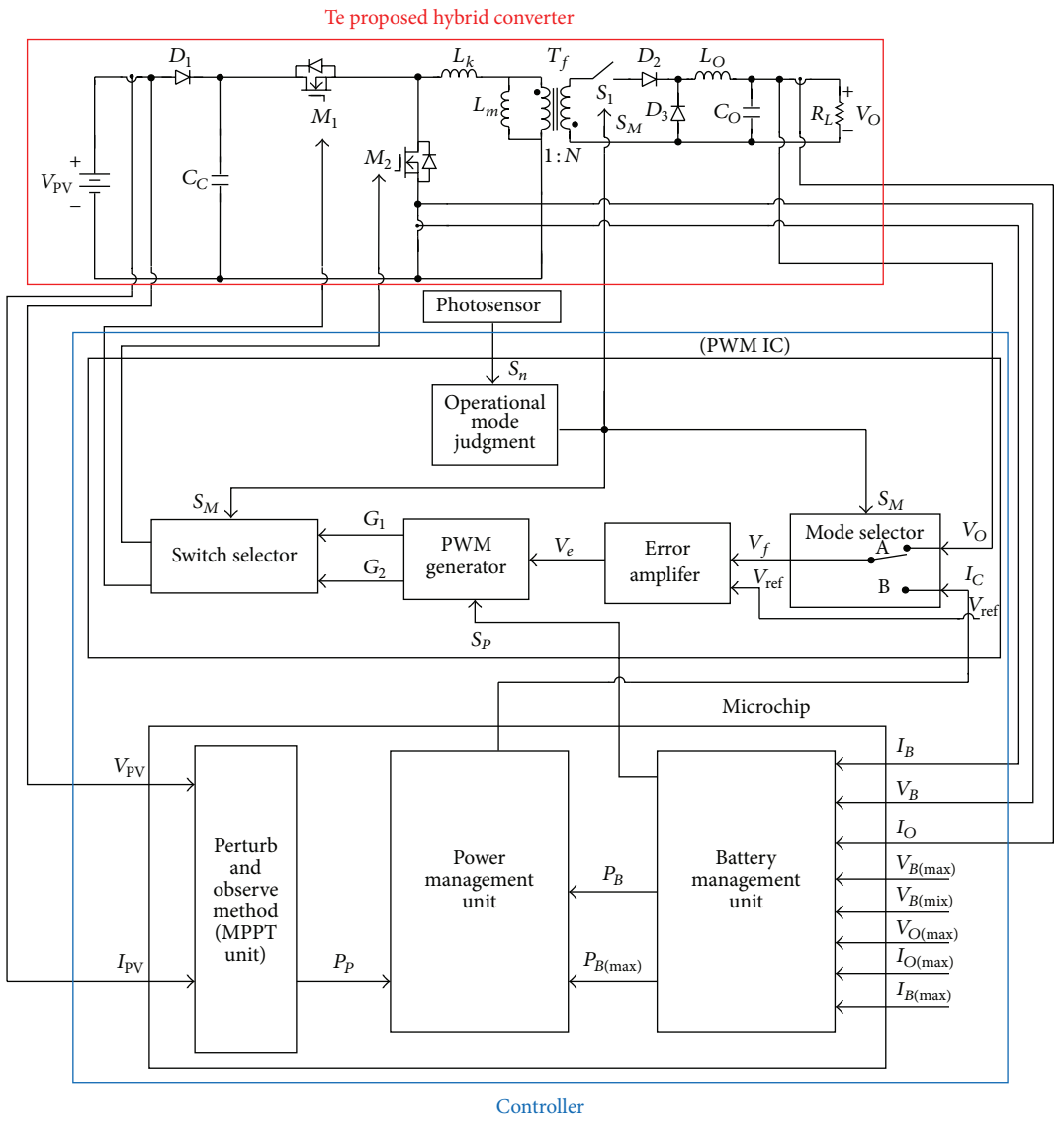

Figure 7: Block diagram of the proposed hybrid converter.

In the following, control algorithms for battery charging and LED driving are briefly described.

4.2.1. Battery Charging. Since the proposed hybrid converter supplies power to load from PV arrays, the proposed one must perform MPPT for PV arrays and battery charging for battery. The MPPT control method and battery charging method are described as follows.

MPPT Algorithm. Since solar cell has a lower output voltage and current, a number of solar cells are connected in series and parallel to form PV arrays for attaining the desired PV voltage and current. Their output characteristic variations depend on ambient temperature and insolation of sun. Figure 8 illustrates *P-V* curve of PV arrays at different insolation of sun, from which it can be seen that each insolation level has a maximum power P_{max} where $P_{max\,1}$ is the most insolation of sun, while $P_{max\,3}$ is the one at the least insolation. Three maximum power point $P_{max\,1} \sim P_{max\,3}$ can be connect by a straight line. The operational area is divided into two areas: A area and B area. When operational point of PV arrays locates in A area, output current I_{PV} of PV arrays is decreased to make the operational point close to its maximum power point (MPP). If operational point is set in B area, current I_{PV} will be increased to operate PV arrays at its MPP.

The proposed power system adopts perturb and observe method to implement MPPT. Its flowchart is shown in Figure 9. In Figure 9, V_n and P_p separately represent their old voltage and power, and P_n ($=V_nI_n$) is its new power. According to flowchart procedures of MPPT using perturb and observe method, first step is to read new voltage V_n and current I_n of PV arrays and then to calculate new PV power P_n. Next step is to judge relationship of P_n and P_p. Since the relationship of P_n and P_p has three different relationships, they are separately

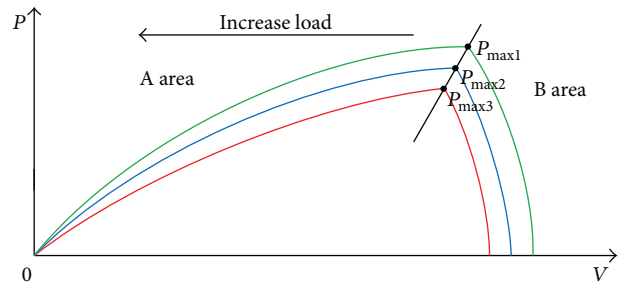

Figure 8: Plot of P-V curve for PV arrays at different isolation of sun.

$P_n > P_p$, $P_n = P_p$, and $P_n < P_p$. Each relationship can be corresponded to the different relationship of V_n and V_p. Therefore, when the relationship of P_n and P_p is decided, next step is to find the relationship of V_n and V_p. According to the relationship of P-V curve of PV arrays, when the relationships of P_n and P_p and V_n an V_p are decided, working point of PV arrays can be specified. When working point of PV arrays locates in A area, power system connected in PV arrays to supply load power must decrease output power to close the distance between working point and MPP of PV arrays. On the other hand, when working point sets in B area, power system must increase output power to make working point to approach MPP of PV arrays. Finally, V_p is replaced by V_n and P_p is also substituted by P_n. The procedure of flowchart returns first step to judge next working point of PV arrays. Moreover, when $P_n = P_P$ and $V_n = V_P$, working point of PV arrays set in the MPP of PV arrays. The maximum power P_P of PV arrays is transferred to power management unit for regulating power of battery charging.

Battery Charging Method. The proposed hybrid converter uses CC charging method to charge battery. According to battery specifications, charging voltage and current are limited for extending its life cycle. Therefore, the power limitation curve for battery charger will be limited. Figure 10 depicts conceptual waveforms of charging current, voltage, and power for battery charger with CC charging method. The battery charging time is from T_0 to T_c. When $t = T_0$, the proposed power system begins to charge battery and battery voltage V_B is at the minimum value $V_{B(\min)}$. When $t = T_c$, battery is charged to its maximum voltage $V_{B(\max)}$. According to limitation of the maximum battery charging current $I_{B(\max)}$, power limitation curve of battery charging can be determined from T_0 to T_c. The charging power of battery follows the power limitation curve for extending its life cycle.

Since power limitation curve of battery has upper and lower values, they are, respectively, $P_{B(\min)}$ $(=V_{B(\min)}I_{B(\max)})$ and $P_{B(\max)}$ $(=V_{B(\max)}I_{B(\max)})$. According to relationship among $P_{PV(\max)}$, $P_{B(\min)}$, and $P_{B(\max)}$, they can be divided into three operational states: $P_{PV(\max)} < P_{B(\min)}$, $P_{B(\min)} \le P_{PV(\max)} < P_{B(\max)}$, and $P_{PV(\max)} > P_{B(\max)}$, as shown in Figure 11. When $P_{PV(\max)} < P_{B(\min)}$, power curve of battery charging follows $P_{PV(\max)}$. When $P_{B(\min)} \le P_{PV(\max)} < P_{B(\max)}$, power limitation curve and $P_{PV(\max)}$ intersects at A point where its intersecting time is T_A. Power curve tracks power limitation curve before $t = t_A$, while it traces $P_{PV(\max)}$ after $t = t_A$, as shown in Figure 11(b). If operational state of $P_{PV(\max)} > P_{B(\max)}$, power curve is regulated by power limitation curve, as shown in Figure 11(c). As mentioned above, battery charging can be operated in a better charging mode.

In order to implement a better battery charging, power management and battery management units are adopted and they are implemented by microchip. In the following, power management and battery management are briefly described.

(1) Power Management. In Figure 7, the controller includes microchip and PWM IC. When the microchip is used to execute power management, its control procedures are depicted in Figure 12. First step is to set $S_P = 0$ and then is to read control signals. The control signals include $V_{O(\max)}$, $V_{B(\max)}$, $V_{B(\min)}$, V_B, I_B, $I_{B(\max)}$, I_O, $I_{O(\max)}$, V_{ref}, and P_P. When control signals are obtained by microchip, next step is to calculate $P_{B(\max)}$ $(=V_B I_{B(\max)})$ and P_B $(=V_B I_B)$. Since P_P, which is attained by MPPT control method, is the maximum output power of PV arrays, when $P_P \ge P_{B(\max)}$ is confirmed, P_{set} is set to equal $P_{B(\max)}$. If $P_P \ge P_{B(\max)}$ is denied, $P_{\text{set}} = P_P$. The P_P is the power command of battery charging. Therefore, power error value ΔP can be determined. It is equal to $(P_{\text{set}} - P_B)$. When ΔP is determined, current command I_C can be obtained. It is equal to $(\Delta P/V_B)$. The current command I_C is sent to PWM IC to determine gate signals G_1 and G_2. Next step is to judge next current command.

(2) Battery Management. In Figure 12, the right hand side of flowchart shows procedures of battery management. When the microchip reads control signals, the procedure of battery management is to judge overcurrent condition. When $I_O \ge I_{O(\max)}$ is confirmed, overcurrent condition of the proposed hybrid converter occurred. When overcurrent condition occurred, signal S_P is set to 1. The S_P is sent to PWM IC to shutdown PWM generator and the proposed hybrid converter is also shutdown. Next step is to judge next current command. Moreover, when $V_O \ge V_{O(\max)}$ (overcharge condition), $V_B \le V_{B(\min)}$ (undercharge condition) and $V_B \ge V_{B(\max)}$ (overcharge condition), the control procedure enters to set $S_P = 1$ and to shutdown the proposed hybrid converter. According to previously describing procedures, battery can be properly controlled to complete a better charging condition.

(3) PWM IC. In the battery charging mode, PWM IC is used to control charging current with CC method. First, photosensor is used to detect insolation level of sun. When insolation is a high level, $S_n = 0$. If insolation is a low level, $S_n = 1$. The signal S_n is sent to operational mode judgment to obtain mode control signal S_M. When $S_M = 0$, the hybrid converter enters battery charging mode. That is, the insolation of sun is at a high level and $S_n = 0$. If $S_M = 1$, the one is in LED driving mode. The signal $S_n = 1$ and insolation is at a low level. The mode control signal S_M is sent to mode selector, switch selector, and switch S_1. When mode selector

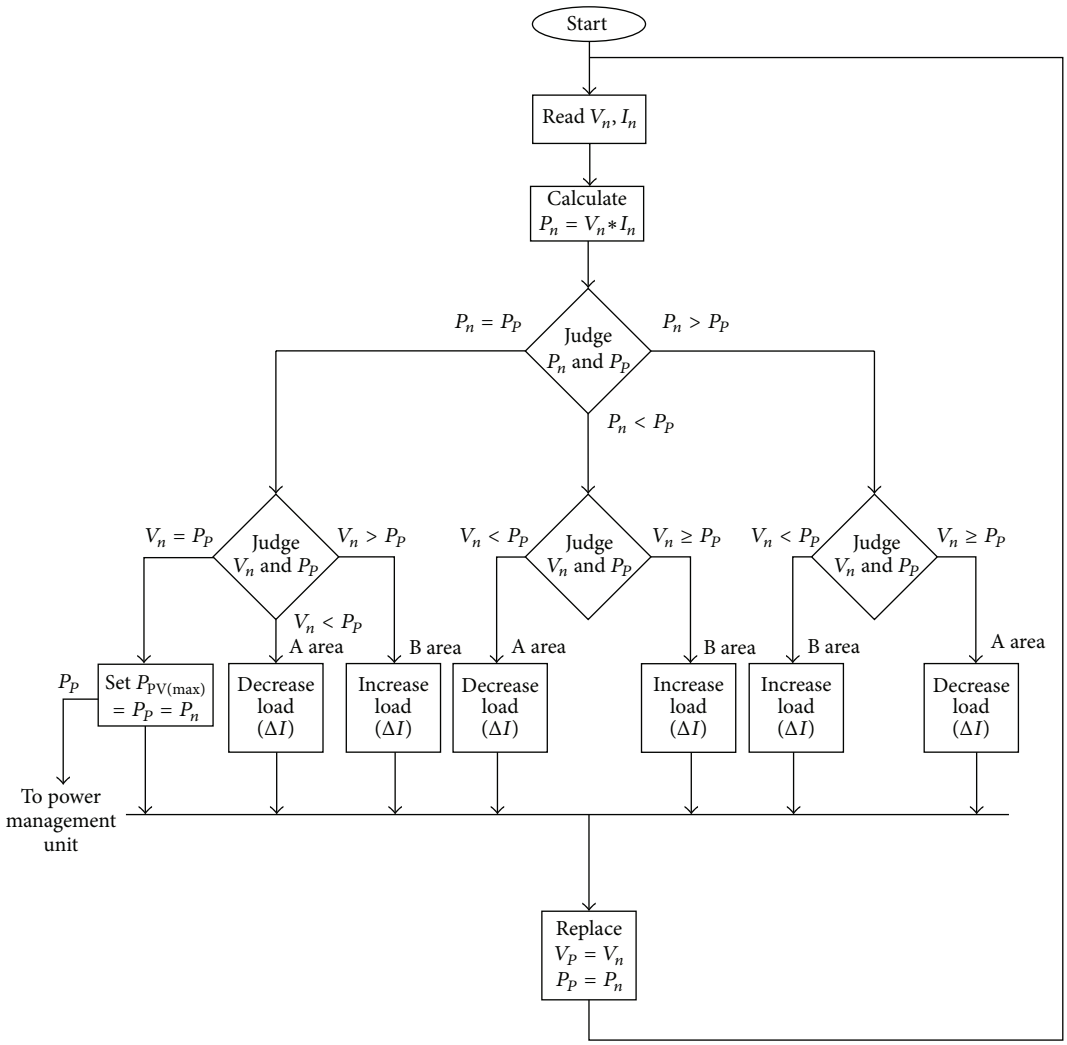

Figure 9: Flowchart of MPPT using perturb and observe method for PV arrays system.

receives $S_M = 0$, the feedback signal V_f is set to equal IC. The feedback signal V_f and reference single V_{ref} are sent to error amplifier to obtain error value V_e. When error value V_e is attained, PWM generator can depend on V_e to determine duty ratios of PWM signals G_1 and G_2. When G_1 and G_2 are specified and $S_M = 0$, switch selector can set that $M_1 = G_1$ and $M_2 = G_2$ to control the charging current I_B of battery. As mentioned above, the proposed hybrid converter can use microchip and PWM IC to achieve battery charging.

4.2.2. LED Driving. The LED driving mode is regarded as battery discharging mode. When operational mode enters LED driving mode, $S_M = 1$. The mode selector can be operated to set $V_f = V_O$. The V_f and V_{ref} are sent to error amplifier to attain V_e. The V_e is through PWM generator to generate signals G_1 and G_2. Since $S_M = 1$, switch selector is controlled by S_M to set $M_1 = G_2$ and $M_2 = G_1$. Therefore, the proposed hybrid converter can depend on duty ratios of gate signals M_1 and M_2 to supply power to LED until battery voltage V_B is equal to or less than $V_{B(\min)}$. When $V_B \leq V_{B(\min)}$, the proposed hybrid converter is shutdown.

5. Experimental Results

In order to verify the circuit analysis and component design of the proposed power system, a prototype, which is composed of a charger and LED driving circuit (discharger), with the following specifications was implemented.

5.1. Buck-Boost Converter (Charger)

(i) Input voltage V_{PV} : DC 17 V~21 V (PV arrays)

(ii) Switching frequency f_{s1} : 250 KHz

(iii) Output voltage V_B : DC 5~7 V (lead-acid battery: 6 V/2.3 Ah)

(iv) Maximum output current $I_{B(\max)}$: 2.3 A.

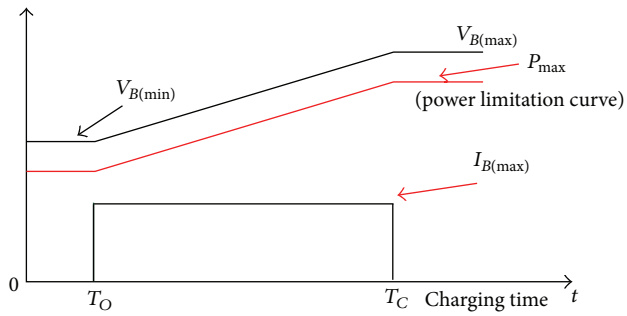

FIGURE 10: Conceptual waveforms of charging current, voltage, and power for battery charger with CC charging method.

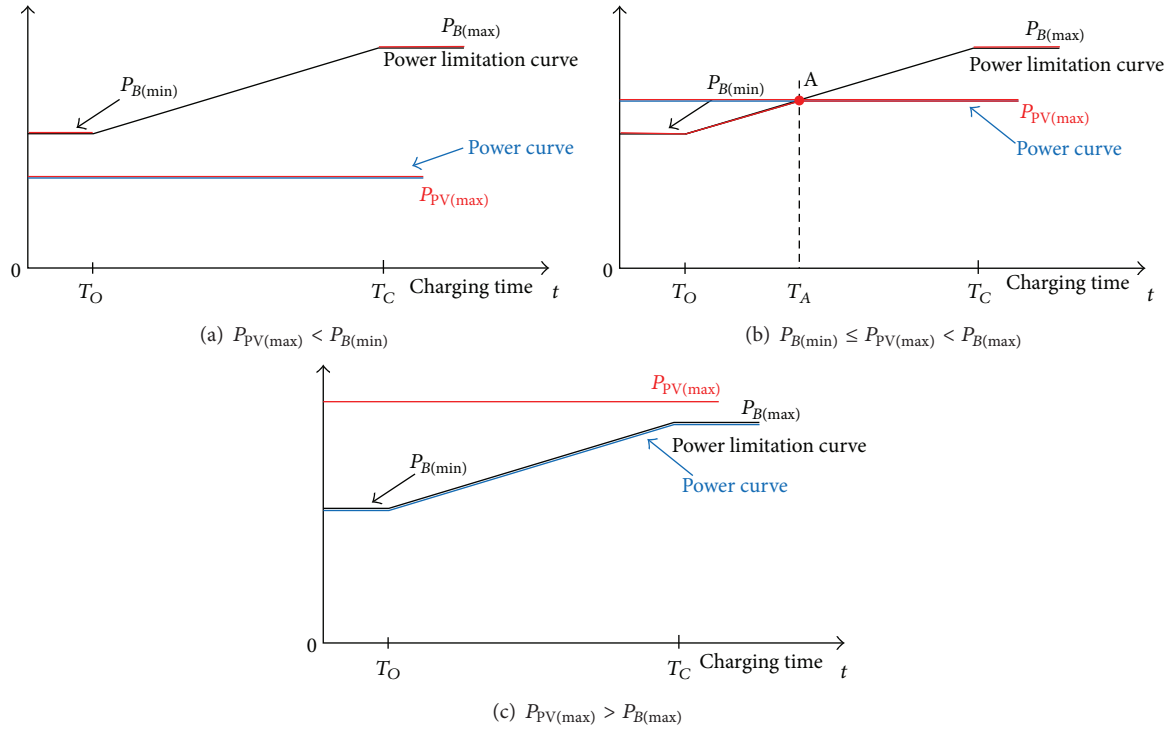

FIGURE 11: Conceptual waveforms of maximum output power of PV arrays and power limitation and power curves of battery from T_O to T_C: (a) $P_{PV(max)} < P_{B(min)}$, (b) $P_{B(min)} \le P_{PV(max)} < P_{B(max)}$, and (c) $P_{PV(max)} > P_{B(max)}$.

5.2. Active Clamp Forward Converter (LED Driving Circuit)

(i) Input voltage V_B : DC 5 V~7 V

(ii) Switching frequency f_{s2} : 250 KHz

(iii) Output voltage V_O : DC 10 V

(iv) Maximum output current $I_{O(max)}$: 2 A.

According to previously specifications and design of the hybrid converter, inductors L_2 and L_m and capacitor C_C can be determined. In (17) illustrated in [23], since inductor L_m must be greater than 7.09 uH under $V_O = 10$ V, $V_B = 7$ V, and $V_{PV} = 17$ V, L_2 is chosen by 40 uH. According to (6) and (22) illustrated in [23], the magnetizing inductor L_m must be greater than 6.8 uH under $N = 5$, $V_B = 7$ V, and $L_2 = 40$ uH. Therefore, magnetizing inductor L_m is determined by 40 uH, while its leakage inductor L_K is obtained by 0.2 uH. Moreover, capacitor C_C can be attained by (29) illustrated in [23]. Its capacitance C_C is 0.22 nF under $N = 5$ and $V_B = 7$ V. Therefore, C_C is chosen by 0.24 uF. The components of power stage in the proposed hybrid converter was determined as follows:

(i) switches M_1, M_2: PSMN005-75B,

(ii) diodes D_1, D_2: UF601,

(iii) transformer T_f: EE-25 core,

(iv) inductor L_2: EE-22 core,

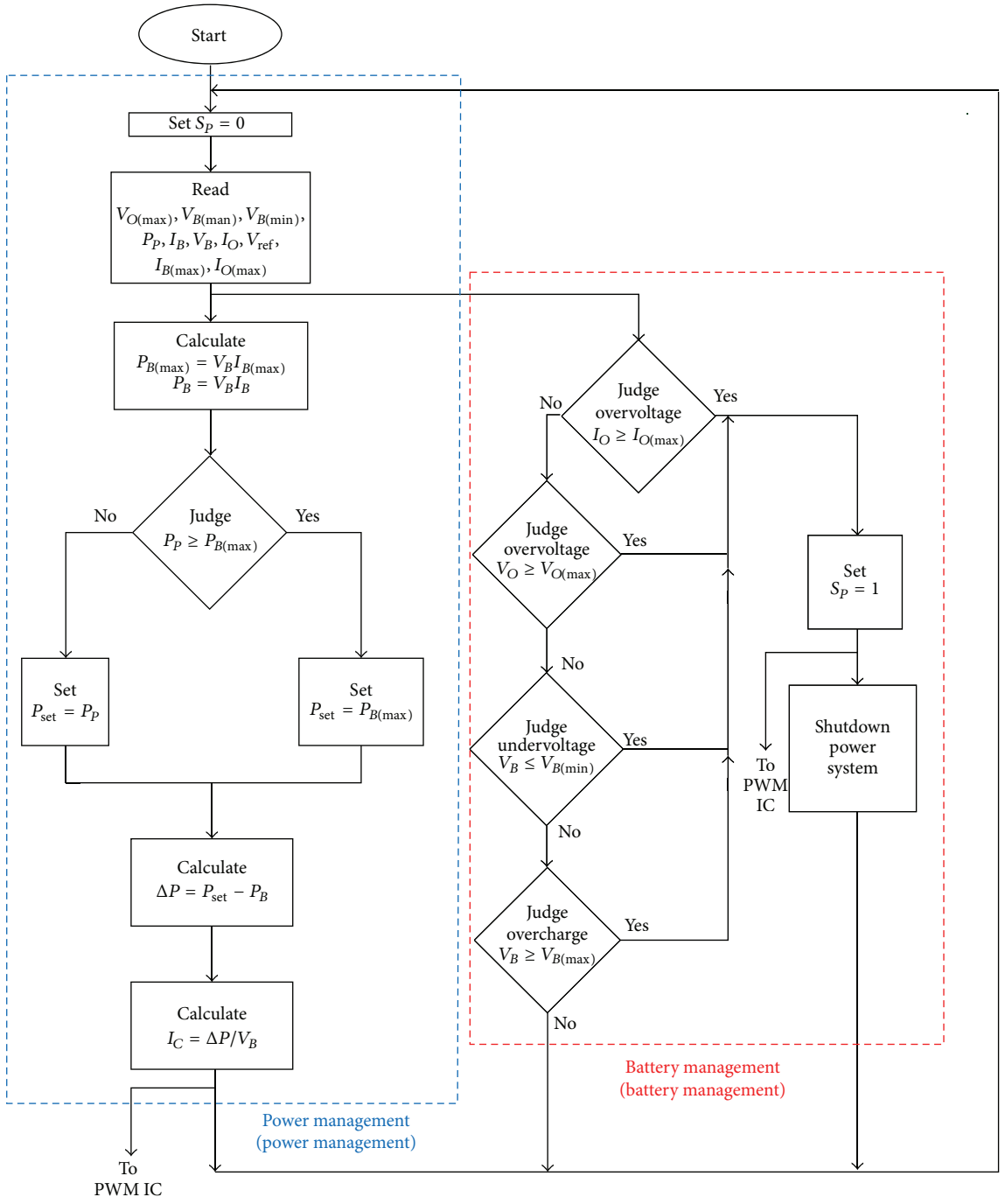

Figure 12: Flowchart of power and battery managements of the proposed hybrid converter.

(v) capacitor C_O: 47 μF/25 V, and

(vi) switch S_1: IRFP540.

Since the charging current I_B of battery can be varied by duty ratio of switch M_1 in buck-boost converter, its value is proportional to duty ratio D_{11}. Figures 13(a) and 13(b), respectively, depict the measured voltage V_{DS} waveform of switch M_1 and current I_B waveform under duty ratio of 0.31 and 0.35, illustrating that the charging current I_B can be increased by duty ratios increase. Measured waveforms of PV arrays current I_{PV} and voltage V_{PV} using the perturb and observe method are illustrated in Figure 14. Figure 14(a) illustrates the MPP of PV arrays at 10 W, while Figure 14(b) depicts that at 20 W. Figure 15 shows the measured battery voltage V_B and current I_B under MPP of PV arrays at 10 W, from which it can be found that the maximum charging

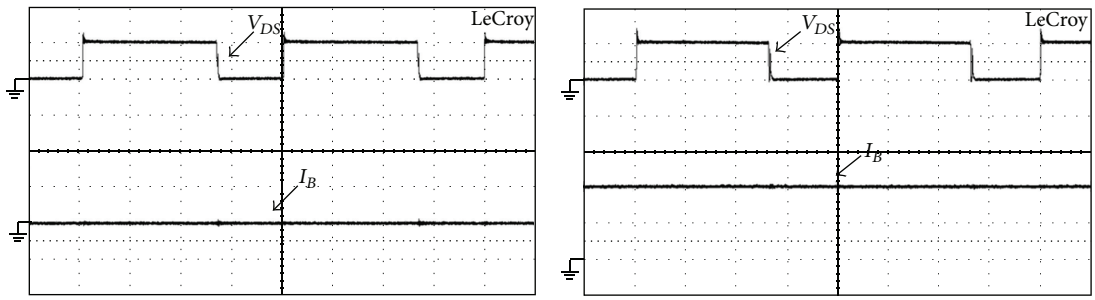

(V_{DS}: 25 V/div, I_{DS}: 500 mA/div, 1 μs/div)

(a)

(V_{DS}: 25 V/div, I_{DS}: 500 mA/div, 1 μs/div)

(b)

Figure 13: Measured voltage V_{DS} waveform of switch M_1 and the charged current I_B waveform operated in duty ratio of (a) 0.31 and (b) 0.35 for working in the charging state.

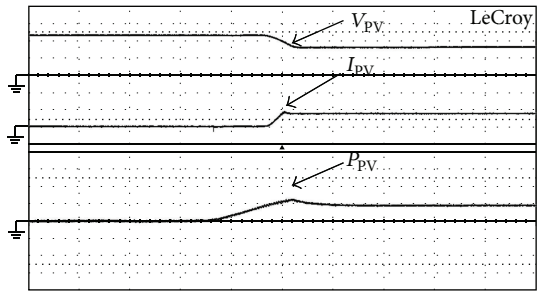

(V_{PV}: 20 V/div, I_{PV}: 2 A/div, P_{PV}: 50 W/div, time: 100 ms/div)

(a)

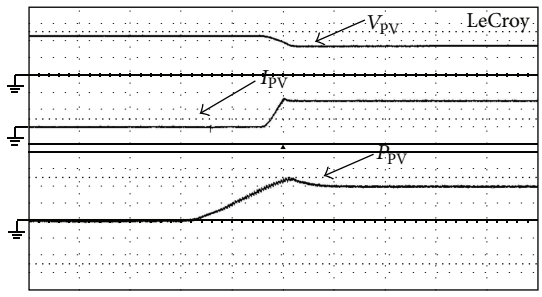

(V_{PV}: 20 V/div, I_{PV}: 2 A/div, P_{PV}: 50 W/div, time: 100 ms/div)

(b)

Figure 14: Measured voltage V_{PV}, current I_{PV}, and power P_{PV} waveforms of PV arrays using the perturb and observe method to track MPPT of arrays (a) under $P_{PV(max)}$ = 10 W and (b) under $P_{PV(max)}$ = 20 W.

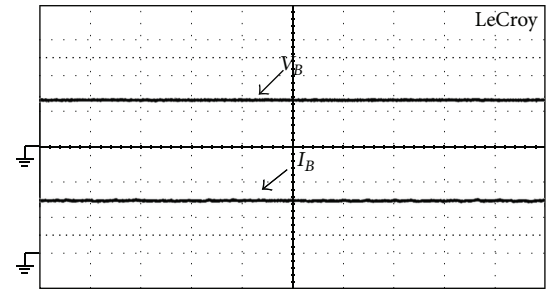

(V_B: 5 V/div, I_B: 1 A/div, time: 10 ms/div)

Figure 15: Measured battery voltage V_B and current I_B waveforms under $P_{PV(max)}$ = 10 W.

current I_B is limited at 1.5 A under battery voltage V_B of 6.5 V due to control of power management.

When the proposed hybrid converter is operated in the discharging state (LED driving state), active clamp forward is in working. Measured voltage V_{DS} and current I_{DS} waveforms of switched M_1 and M_2 are, respectively, illustrated in Figures 16 and 17. Figures 16(a) and 16(b) show those waveforms under 20% of full load, while Figures 17(a) and 17(b) depict those waveforms under full load. From Figures 16 and 17, it can be seen that switches M_1 and M_2 are operated with ZVS at turn-on transition. Comparison of conversion efficiency between forward converter with hard-switching circuit and with the proposed active clamp circuit from light load to heavy load is depicted in Figure 18, from which it can be found that the efficiency of the proposed converter is higher than that of hard-switching one. Its maximum efficiency is 90% under 80% of full load and its efficiency is 83% under full load. Figure 19 illustrates step-load change between 20% of full load and full load, illustrating that the voltage regulation V_O has been limited within ±2%. From experimental results, it can be found that the proposed hybrid converter is suitable for electronic sign applications.

6. Conclusion

In this paper, the buck-boost converter combined with active clamp forward converter to form the proposed hybrid converter is used to implement battery charger and driving LED. Circuit derivation of the hybrid converter with switch integration technique is presented in this paper to reduce component counts. Operational principle, steady-state analysis, and design of the proposed hybrid converter have been described in detail. From efficiency comparison between forward converter with hard-switching circuit and with the proposed active clamp circuit, the proposed active clamp converter can yield higher efficiency. An experimental

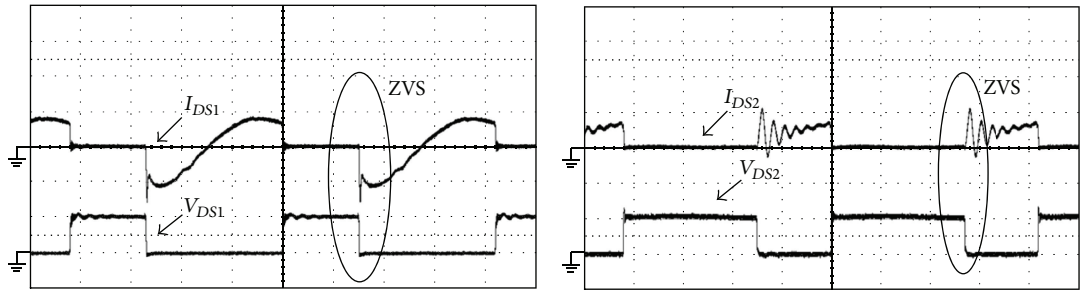

(V_{DS1}: 10 V/div, I_{DS1}: 4 A/div, 1 μs/div) (a)

(V_{DS2}: 10 V/div, I_{DS2}: 4 A/div, 1 μs/div) (b)

FIGURE 16: Measured voltage V_{DS} and current I_{DS} waveforms of (a) switch M_1 and (b) switch M_2 for working under 20% of full load.

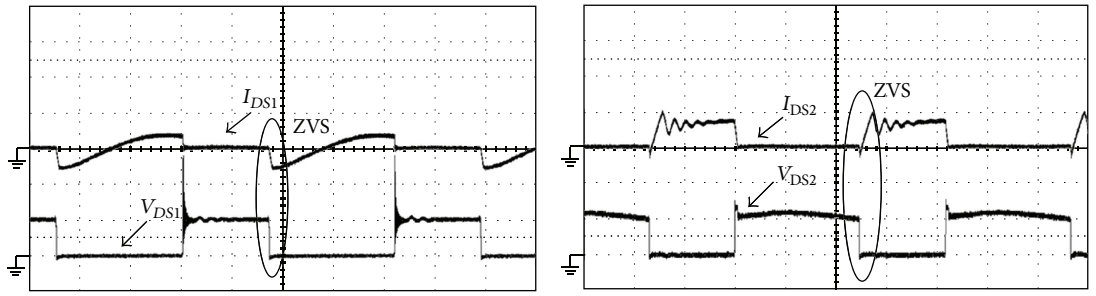

(V_{DS1}: 10 V/div, I_{DS2}: 15 A/div, 1 μs/div) (a)

(V_{DS2}: 10 V/div, I_{DS2}: 15 A/div, 1 μs/div) (b)

FIGURE 17: Measured voltage V_{DS} and current I_{DS} waveforms of (a) switch M_1 and (b) switch M_2 for working under full load.

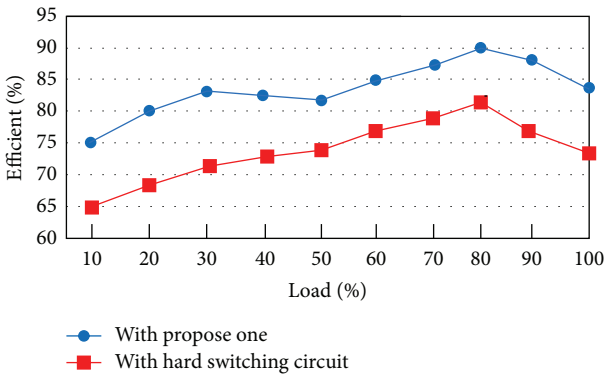

FIGURE 18: Comparison conversion efficiency between the conventional hard-switching forward converter and the proposed one from light load to heavy load for working in the discharging state.

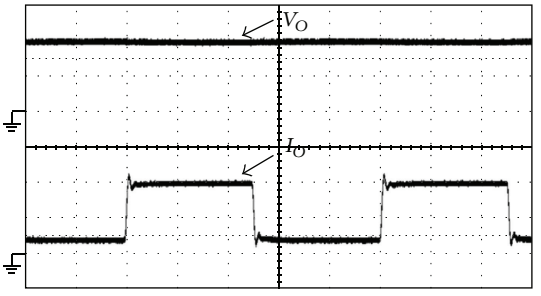

(V_O : 5 V/div, I_O : 1 A/div, 500 μs/div)

FIGURE 19: Output voltage V_O and output current I_O under step-load charges between 30% and 100% of full load of the proposed forward converter operated in the discharging state.

prototype for a battery charger for lead-acid battery of 6 V/2.3 Ah and discharger for LED driving under 10 V/2 A has been built and evaluated, achieving the maximum efficiency of 90% under 80% of full load and verifying the feasibility of the proposed hybrid converter. Moreover, constant current charging method, MPPT with perturb and observe method, and power management have been implemented by microchip and PWM IC.

Conflict of Interests

The authors declare that there is no conflict of interests regarding the publication of this paper.

References

[1] Y. Jiang, A. W. Leung, J. Xiang, and C. Xu, "LED light-activated hypocrellin B induces mitochondrial damage of ovarian cancer cells," *International Journal of Photoenergy*, vol. 2012, Article ID 186752, 5 pages, 2012.

[2] C.-H. Liu, C.-Y. Hsieh, Y.-C. Hsieh, T.-J. Tai, and K.-H. Chen, "SAR-controlled adaptive off-time technique without sensing resistor for achieving high efficiency and accuracy LED lighting system," *IEEE Transactions on Circuits and Systems I*, vol. 57, no. 6, pp. 1384–1394, 2010.

[3] C. C. Chen, C.-Y. Wu, and T.-F. Wu, "LED back-light driving system for LCD panels," in *Proceedings of The Applied Power Electronics Conference and Exposition*, pp. 19–23, 2006.

[4] S.-Y. Tseng and C.-T. Tsai, "Photovoltaic power system with an interleaving boost converter for battery charger applications," *International Journal of Photoenergy*, vol. 2012, Article ID 936843, 15 pages, 2012.

[5] J.-H. Park and B.-H. Cho, "Nonisolation soft-switching buck converter with tapped-inductor for wide-input extreme step-down applications," *IEEE Transactions on Circuits and Systems I*, vol. 54, no. 8, pp. 1809–1818, 2007.

[6] K. Mehran, D. Giaouris, and B. Zahawi, "Stability analysis and control of nonlinear phenomena in boost converters using model-based Takagi-Sugeno fuzzy approach," *IEEE Transactions on Circuits and Systems I*, vol. 57, no. 1, pp. 200–212, 2010.

[7] B. Bryant and M. K. Kazimierczuk, "Open-loop power-stage transfer functions relevant to current-mode control of boost PWM converter operating in CCM," *IEEE Transactions on Circuits and Systems I*, vol. 52, no. 10, pp. 2158–2164, 2005.

[8] M. R. Yazdani, H. Farzanehfard, and J. Faiz, "EMI analysis and evaluation of an improved ZCT flyback converter," *IEEE Transactions on Power Electronics*, vol. 26, no. 8, pp. 2326–2334, 2011.

[9] K. I. Hwu and T. J. Peng, "A novel buck-boost converter combining KY and buck converters," *IEEE Transactions on Power Electronics*, vol. 27, no. 5, pp. 2236–2241, 2012.

[10] F. Xie, R. Yang, and B. Zhang, "Bifurcation and border collision analysis of voltage-mode-controlled flyback converter based on total ampere-turns," *IEEE Transactions on Circuits and Systems I*, vol. 58, no. 9, pp. 2269–2280, 2011.

[11] B.-R. Lin and H.-Y. Shih, "Implementation of a parallel zero-voltage switching forward converter with less power switches," *IET Power Electronics*, vol. 4, no. 2, pp. 248–256, 2011.

[12] D. Wang, X. He, and J. Shi, "Design and analysis of an interleaved flybackforward boost converter with the current autobalance characteristic," *IEEE Transactions on Power Electronics*, vol. 25, no. 2, pp. 489–498, 2010.

[13] T.-F. Wu and T.-H. Yu, "Unified approach to developing single-stage power converters," *IEEE Transactions on Aerospace and Electronic Systems*, vol. 34, no. 1, pp. 211–223, 1998.

[14] K. I. Hwu, W. C. Tu, and C. R. Wang, "Photovoltaic energy conversion system constructed by high step-up converter with hybrid maximum power point tracking," *International Journal of Photoenergy*, vol. 2013, Article ID 275210,, 9 pages, 2013.

[15] A. Braunstein and Z. Zinger, "On the dynamic optimal coupling of a solar cell array to a load and storage batteries," *IEEE transactions on Power Apparatus and Systems*, vol. 100, no. 3, pp. 1183–1188, 1981.

[16] A. S. Weddell, G. V. Merrett, and M. A.-H. Bashir, "Photovoltaic sample-and-hold circuit enabling MPPT indoors for low-power systems," *IEEE Transaction on Circuits and Systems*, vol. 59, no. 6, pp. 1196–1204, 2012.

[17] S. M. M. Wolf and J. H. R. Enslin, "Economical, PV maximum power point tracking regulator with simplistic controller," in *Proceedings of the EEE 24th Annual Power Electronics Specialist Conference*, pp. 581–587, June 1993.

[18] C.-L. Shen and S.-H. Yang, "Multi-input converter with MPPT feature for wind-PV power generation system," *International Journal of Photoenergy*, vol. 2013, Article ID 129254, 13 pages, 2013.

[19] R. Leyva, C. Olalla, H. Zazo et al., "MPPT based on sinusoidal extremum-seeking control in PV generation," *International Journal of Photoenergy*, vol. 2012, Article ID 672765, 7 pages, 2012.

[20] N. Onat, "Recent developments in maximum power point tracking technologies for photovoltaic systems," *International Journal of Photoenergy*, vol. 2010, Article ID 245316, 11 pages, 2010.

[21] K. H. Hussein, I. Muta, T. Hoshino, and M. Osakada, "Maximum photovoltaic power tracking: an algorithm for rapidly changing atmospheric conditions," *IEE Proceedings: Generation, Transmission and Distribution*, vol. 142, no. 1, pp. 59–64, 1995.

[22] S. R. Rajwade, K. Auluck, J. B. Phelps, K. G. Lyon, J. T. Shaw, and E. C. Kan, "A ferroelectric and charge hybrid nonvolatile memory—Part II: experimental validation and analysis," *IEEE Transactions on Electron Devices*, vol. 59, no. 2, pp. 450–458, 2012.

[23] S. Y. Tseng, H. Y. Wang, and C. C. Chen, "PV power system using hybrid converter for LED indictor applications," *Energy Conversion and Management*, vol. 75, pp. 761–772, 2013.